

Wide-bandwidth continuously tunable optical delay line using silicon microring resonators

Jaime Cardenas,¹ Mark A. Foster,³ Nicolás Sherwood-Droz,¹ Carl B. Poitras,¹ Hugo L. R. Lira,¹ Beibei Zhang,⁴ Alexander L. Gaeta,³ Jacob B. Khurgin,⁴ Paul Morton,⁵ and Michal Lipson^{1,2*}

¹*School of Electrical and Computer Engineering, Cornell University, Ithaca, NY, USA*

²*Kavli Institute at Cornell for Nanoscale Science, Cornell University, Ithaca, NY, USA*

³*School of Applied and Engineering Physics, Cornell University, Ithaca, NY, USA*

⁴*Department of Electrical and Computer Engineering, Johns Hopkins University, Baltimore, MD, USA*

⁵*Morton Photonics, West Friendship, MD, USA*

*ml292@cornell.edu

Abstract: We demonstrate a distortion free tunable optical delay as long as 135 ps with a 10 GHz bandwidth using thermally tuned silicon microring resonators in the novel balanced configuration. The device is simple, easy to control and compact measuring only 30 μm wide by 250 μm long.

©2010 Optical Society of America

OCIS codes: (230.3120) Integrated optics devices; (230.7370) Waveguides; (250.5300) Photonic integrated circuits.

References and links

1. R. W. Boyd, D. J. Gauthier, and A. L. Gaeta, "Applications of slow light in telecommunications," *Opt. Photon. News* **17**(4), 18–23 (2006).
2. J. L. Corral, J. Marti, J. M. Fuster, and R. I. Laming, "True time-delay scheme for feeding optically controlled phased-array antennas using chirped-fiber gratings," *Photon. Technol. Lett.* **9**(11), 1529–1531 (1997).
3. A. E. Willner, B. Zhang, L. Zhang, L. Yan, and I. Fazal, "Optical signal processing using tunable delay elements based on slow light," *IEEE J. Sel. Top. Quantum Electron.* **14**(3), 691–705 (2008).
4. Y. A. Vlasov, M. O'Boyle, H. F. Hamann, and S. J. McNab, "Active control of slow light on a chip with photonic crystal waveguides," *Nature* **438**(7064), 65–69 (2005).
5. D. O'Brien, A. Gomez-Iglesias, M. D. Settle, A. Michaeli, M. Salib, and T. F. Krauss, "Tunable optical delay using photonic crystal heterostructure nanocavities," *Phys. Rev. B* **76**(11), 115110 (2007).
6. T. Baba, "Slow light in photonic crystals," *Nat. Photonics* **2**(8), 465–473 (2008).
7. C. Yu, T. Luo, L. Zhang, and A. E. Willner, "Data pulse distortion induced by a slow-light tunable delay line in optical fiber," *Opt. Lett.* **32**(1), 20–22 (2007).
8. Z. Shi, and R. W. Boyd, "Discretely tunable optical packet delays using channelized slow light," *Phys. Rev. A* **79**(1), 013805 (2009).
9. J. E. Sharping, Y. Okawachi, and A. L. Gaeta, "Wide bandwidth slow light using a Raman fiber amplifier," *Opt. Express* **13**(16), 6092–6098 (2005).
10. Y. Okawachi, M. A. Foster, J. E. Sharping, A. Gaeta, Q. Xu, and M. Lipson, "All-optical slow-light on a photonic chip," *Opt. Express* **14**(6), 2317–2322 (2006).
11. M. S. Rasras, C. K. Madsen, M. A. Cappuzzo, E. Chen, L. T. Gomez, E. J. Laskowski, A. Griffin, A. Wong-Foy, A. Gasparyan, A. Kasper, J. Le Grange, and S. S. Patel, "Integrated resonance-enhanced variable optical delay lines," *IEEE Photon. Technol. Lett.* **17**(4), 834–836 (2005).
12. C. G. H. Roeloffzen, L. Zhuang, R. G. Heideman, A. Borreman, and W. van Etten, "Ring resonator-based tunable optical delay line in LPCVD waveguide technology," *Proc. IEEE/LEOS Benelux Chapter*, 2005.
13. Q. Xu, J. Shakya, and M. Lipson, "Direct measurement of tunable optical delays on chip analogue to electromagnetically induced transparency," *Opt. Express* **14**(14), 6463–6468 (2006).
14. F. Morichetti, A. Melloni, A. Breda, A. Canciamilla, C. Ferrari, and M. Martinelli, "A reconfigurable architecture for continuously variable optical slow-wave delay lines," *Opt. Express* **15**(25), 17273–17282 (2007).
15. F. Morichetti, A. Melloni, C. Ferrari, and M. Martinelli, "Error-free continuously-tunable delay at 10 Gbit/s in a reconfigurable on-chip delay-line," *Opt. Express* **16**(12), 8395–8405 (2008).
16. J. Yang, N. K. Fontaine, Z. Pan, A. O. Karalar, S. S. Djordjevic, C. Yang, W. Chen, S. Chu, B. E. Little, and S. J. B. Yoo, "Continuously tunable, wavelength-selective buffering in optical packet switching networks," *IEEE Photon. Technol. Lett.* **20**(12), 1030–1032 (2008).
17. N. K. Fontaine, J. Yang, Z. Pan, S. Chu, W. Chen, B. E. Little, and S. J. Ben Yoo, "Continuously Tunable Optical Buffering at 40 Gb/s for Optical Packet Switching Networks," *J. Lightwave Technol.* **26**(23), 3776–3783 (2008).

18. Z. Hu, J. Sun, L. Liu, and J. Wang, "All-optical tunable delay line based on wavelength conversion in semiconductor optical amplifiers and dispersion in dispersion-compensating fiber," *Appl. Phys. B* **91**(3-4), 421–424 (2008).
19. Y. Okawachi, M. A. Foster, X. Chen, A. C. Turner-Foster, R. Salem, M. Lipson, C. Xu, and A. L. Gaeta, "Large tunable delays using parametric mixing and phase conjugation in Si nanowaveguides," *Opt. Express* **16**(14), 10349–10357 (2008).
20. Y. Dai, X. Chen, Y. Okawachi, A. C. Turner-Foster, M. A. Foster, M. Lipson, A. L. Gaeta, and C. Xu, "1 microsecond tunable delay using parametric mixing and optical phase conjugation in Si waveguides," *Opt. Express* **17**(9), 7004–7010 (2009).
21. F. Xia, L. Sekaric, and Y. Vlasov, "Ultra-compact optical buffers on a silicon chip," *Nat. Photonics* **1**(1), 65–71 (2007).
22. J. B. Khurgin, "Optical buffers based on slow light in EIT media and coupled resonator structures – comparative analysis," *J. Opt. Soc. Am. B* **22**(5), 1062–1074 (2005).
23. J. B. Khurgin, "Dispersion and loss limitations on the performance of optical delay lines based on coupled resonator structures," *Opt. Lett.* **32**(2), 133–135 (2007).
24. C. K. Madsen, "Subband all-pass filter architectures with application to dispersion and dispersion-slope compensation and continuously variable delay lines," *J. Lightwave Technol.* **21**(10), 2412–2420 (2003).
25. L. Zhang, T. Luo, C. Yu, W. Zhang, and A. E. Willner, "Pattern dependence of data distortion in slow-light elements," *J. Lightwave Technol.* **25**(7), 1754–1760 (2007).
26. A. E. Willner, B. Zhang, L. Zhang, L. Yan, and I. Fazal, "Optical signal processing using tunable delay elements based on slow light," *IEEE J. Sel. Top. Quantum Electron.* **14**(3), 691–705 (2008).
27. J. B. Khurgin, and P. A. Morton, "Tunable wideband optical delay line based on balanced coupled resonator structures," *Opt. Lett.* **34**(17), 2655–2657 (2009).
28. N. Sherwood-Droz, H. Wang, L. Chen, B. G. Lee, A. Biberman, K. Bergman, and M. Lipson, "Optical 4x4 hitless silicon router for optical networks-on-chip (NoC)," *Opt. Express* **16**(20), 15915–15922 (2008).
29. V. R. Almeida, C. A. Barrios, R. R. Panepucci, and M. Lipson, "All-optical control of light on a silicon chip," *Nature* **431**(7012), 1081–1084 (2004).

1. Introduction

On-chip tunable delays have applications in data buffering, signal processing, and phased array antennae [1–3]. Different approaches for delays such as photonic crystals [4–6], stimulated Brillouin scattering (SBS) [7, 8], stimulated Raman scattering (SRS) [9, 10], coupled microring resonators [11–17], and wavelength conversion and dispersion [18–20] have been demonstrated. However, these approaches either require high precision fabrication (such as in the photonic crystal case) or rely on large devices (in the case of on-chip SBS, SRS, and wavelength conversion and dispersion).

Compact long delays can be achieved in ring resonators however in these structures the delay is fixed and is limited in bandwidth [21]. This limitation is because these delays rely on high finesse, and therefore inevitably introduce higher order group delay dispersion [22, 23], which limits the bandwidth. One powerful technique to reduce data distortion and increase bandwidth in resonance based delay lines is operating away from the resonance peak [11, 16, 17, 24–27], which sacrifices maximum delay. This technique has been implemented using stimulated Brillouin scattering [25, 26] and thermally tuned silica based microrings [11, 16, 17]. However, the silica based structures are based on large radius rings (an inherent limitation of the silica based platform), from a few hundred microns up to a millimeter. Furthermore, the methods used in [11,16,17] require individual controls of both resonant frequencies and coupling coefficients of a large number of resonators.

In this paper we demonstrate a delay scheme using compact silicon-based microring resonators for enabling high bandwidth and continuous tunability based on the balanced side-coupled integrated spaced sequence of resonators (SCISSOR) structure [27].

2. Balanced SCISSOR Concept and Simulations

The Balanced SCISSOR structure used in this work consists of two sets of identical racetrack shaped microring resonators, which can be on opposite sides of the bus waveguides, as shown in Fig. 1a. The racetrack microrings are characterized by a bend radius of 7 μm and straight sections of 7.5 μm , for an overall circumference of 59 μm . The group index is approximately 4.1, and the coupling coefficient is approximately 0.35. The device is designed to operate in

the TE polarization. If all the rings are at the same resonant frequency, as shown in the delay spectra in Fig. 1b (I), a significant group delay of about 25 ps per ring can be attained. However, this delay has a narrow bandwidth. To expand the bandwidth, as proposed in [27], the resonant frequencies of the resonators are shifted by a small amount $\Delta\omega$ from the central resonance frequency ω_r ; half of the rings are blue shifted and the other half are red shifted, as shown in Fig. 1b (II), with the resulting group delay spectrum shown in Fig. 1b (III). This easy-to-control arrangement, requiring only two independent controls for each of the two sets of rings, reduces the third and higher orders of group delay dispersion [27], as evidenced by the wide spectral regions with essentially flat and ripple-free group delay (see Fig. 2). The resonances of the rings are changed symmetrically about the central resonant frequency ω_r , which is also the operating frequency of the overall structure and remains constant while the group delay is varied. The spectral width of the structure broadens, increasing its bandwidth, as the resonance frequency detuning from ω_r is increased (i.e. the difference in frequency between the rings' resonance frequency and the operating frequency). As shown in Fig. 2b, the third order group delay dispersion crosses zero at a resonance detuning of 7.56 GHz and remains quite low for larger detunings. From Ref. 27, the relationship between delay and

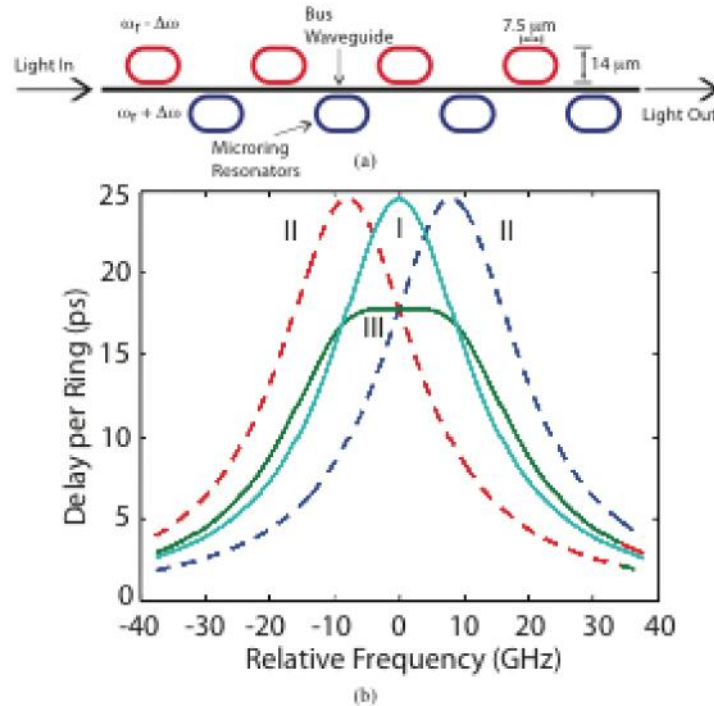


Fig. 1. (a) Tunable delay line structure with overall central frequency ω_r . In order to tune the delay, the resonances of the red (upper) rings are red shifted by increasing the refractive index of the ring, while the resonances of the blue (lower) rings are blue shifted by decreasing the refractive index of the rings. (b) Simulated delay spectra of balanced SCISSOR structure from (a): (I) delay spectra with all rings aligned to ω_r ; (II) delay spectra of red and blue shifted rings; (III) delay spectra for complete device.

resonance detuning, presented here for completeness, is given by

$$\Delta T(\omega) = \sum_{n=1}^N \frac{k^2 \tau}{1 + \rho^2 - 2 \cos(\omega - \omega_n)}$$

where τ is the round trip time, κ is the coupling coefficient, and $\rho = \sqrt{1 - \kappa^2}$.

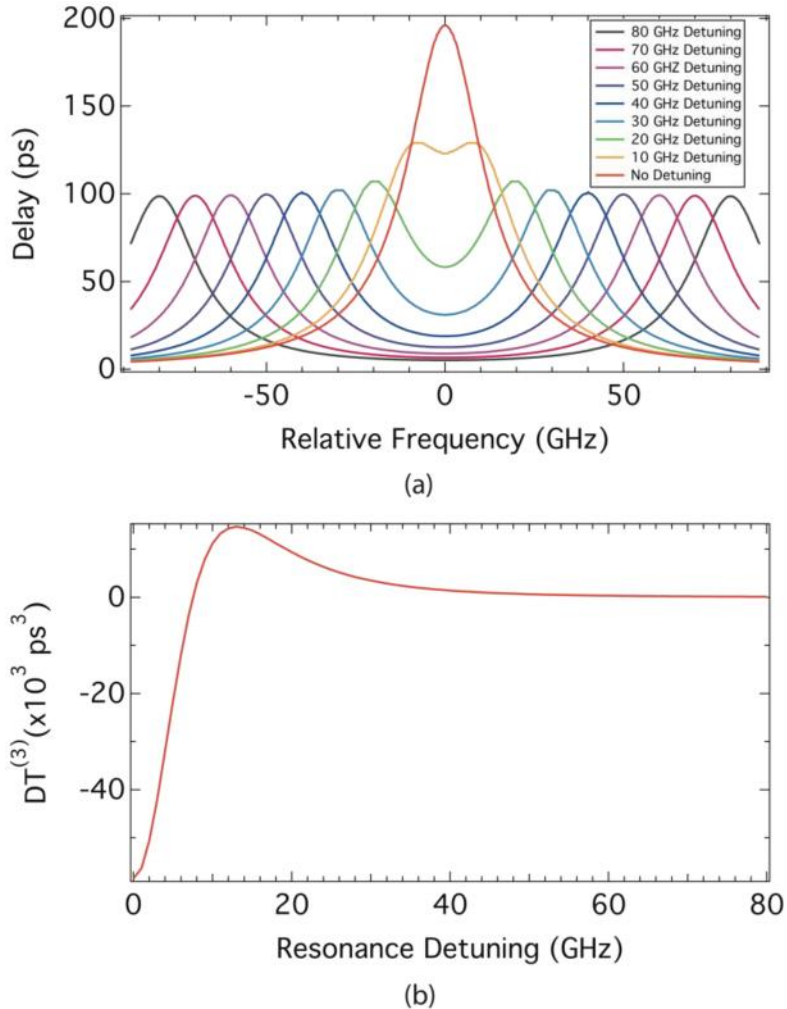


Fig. 2. Balanced SCISSOR simulations calculated using the equations derived in Ref. 27. (a) Delay spectrum as a function of frequency relative to the device's operating frequency. No ripple is observed in the spectrum. (b) Third order delay dispersion as a function of resonance detuning. The simulations show that third order delay dispersion can be cancelled using the Balanced SCISSOR. For larger resonance detuning, the third order delay dispersion remains low.

3. Device fabrication

We fabricate the device using standard CMOS fabrication processes. The fabrication starts with a silicon-on-insulator (SOI) substrate with a 250 nm thick device layer and a 3 μm buried oxide. A silicon dioxide etch mask is deposited via plasma enhanced chemical vapor deposition (PECVD) and the device is patterned using electron beam lithography on Ma-N 2403 resist. To improve adhesion and prevent delamination of the Ma-N 2403 resist, we use Surpass 3000, an adhesion promoter, before spinning the resist. We etch the silicon dioxide mask in a reactive ion etcher (RIE) using fluorine chemistry. After stripping the resist, the silicon is etched in an inductively coupled plasma reactive ion etcher using chlorine chemistry. We deposit 300 nm of silicon dioxide in a low pressure chemical vapor deposition (LPCVD) reactor. This deposition technique is highly conformal and fills in the gaps between the microrings and the bus waveguide. To complete the cladding, 700 nm of silicon dioxide

are deposited via PECVD. The heaters are fabricated directly above the rings by thermal evaporation of 200 nm of chrome using a lift-off process [28]. Finally, gold contact pads are made with thermal evaporation and lift-off (see Fig. 3).

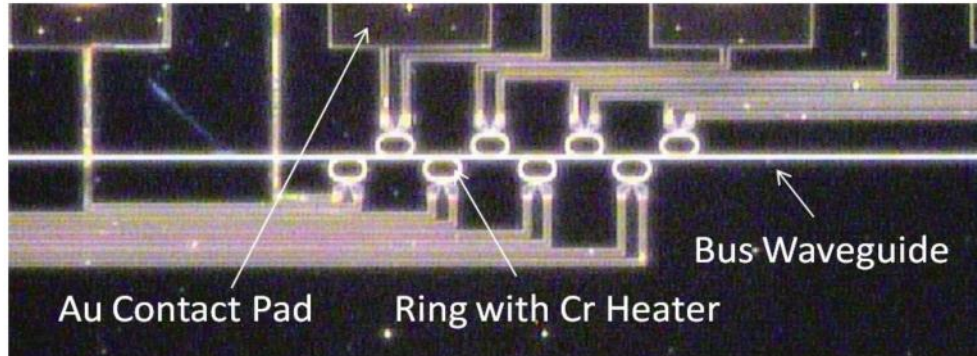


Fig. 3. Microscope image showing the fabricated structure. The heaters are located directly above the rings.

The fabricated SCISSOR device consists of eight rings using a racetrack configuration for low loss coupling with the bus waveguide (see Fig. 3). The rings have circular sections with a radius of $7\ \mu\text{m}$ and straight sections of $7.5\ \mu\text{m}$ long (Fig. 1). The coupling gap between the ring and the bus waveguide is $200\ \text{nm}$. The chrome heaters are $1\ \mu\text{m}$ wide. The fabricated device is $30\ \mu\text{m}$ in width and $250\ \mu\text{m}$ in length, measured from where the rings begin to where they end. The contact pads are $100\ \mu\text{m} \times 100\ \mu\text{m}$ with a $200\ \mu\text{m}$ pitch and are designed to match the probes used to contact the device.

4. Experimental results

We test the device with a continuous 10 Gbps NRZ pattern of 1010111001000110 generated by modulating a tunable laser set at the device's operating wavelength using an electro-optic intensity modulator. Following the modulator, the signal is sent through a second polarization controller, which is used to ensure that the TE polarization is coupled into the SCISSOR device. One percent of the output from the SCISSOR device is sent to an optical spectrum analyzer (OSA) for monitoring. The remaining output is amplified with an EDFA before being passed through a bandpass filter to reduce the ASE noise added by the EDFA. We use another one percent tap to monitor the power arriving at the receiver, which includes a built-in limiting amplifier. One output of the receiver is connected to a sampling oscilloscope and the other output is connected to the receive section of the BERT. The clock output from the pattern generator is used to trigger the sampling oscilloscope and BERT to synchronize the signals and measure the delay and bit error rate (BER) from the device (Fig. 4). The typical fiber coupling loss is 14 dB including the tapered fiber to chip loss, the waveguide propagation loss, and the loss from the microscope objective used to collect the device's output back to a fiber. The coupling loss of the device could be reduced to approximately 3 dB by optimizing the input and output coupling nanotapers [29].

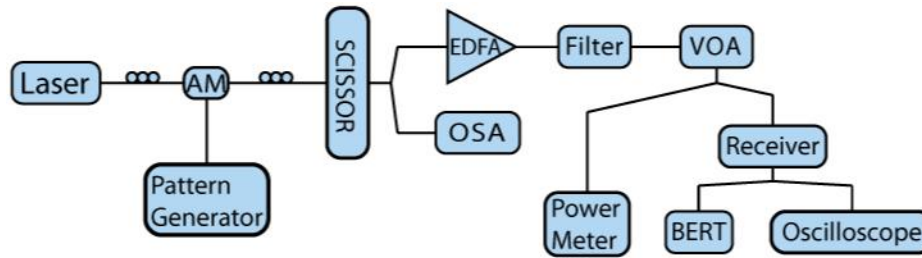


Fig. 4. Test setup schematic. AM: Amplitude modulator; VOA: Variable Optical Attenuator.

The microring resonances, and hence the delay, are tuned using the thermal heaters. Using the thermo-optic effect, the resonances can only be red-shifted, therefore we bias all the resonators with a red shift to the operating wavelength, which then allows us to both blue-shift (by reducing the voltage) and red-shift (by increasing the voltage) the resonances from this operating point. In order to tune the resonances precisely for the balanced SCISSOR operation, the resonance shift vs. applied voltage to the heaters was characterized for all eight rings (Fig. 5). Since we only need to shift the resonances by less than one nanometer, we linearize the curve for each ring about the operating wavelength of the delay. With the slope of these curves, we determine the voltage change required to shift the resonances of the individual rings to achieve the different delays. In practice, additional resistors can be placed in parallel with the heater and trimmed as needed to deliver equal power to all heaters, thus needing only two driving voltages: one to drive all the red detuned rings and one to drive all the blue detuned rings.

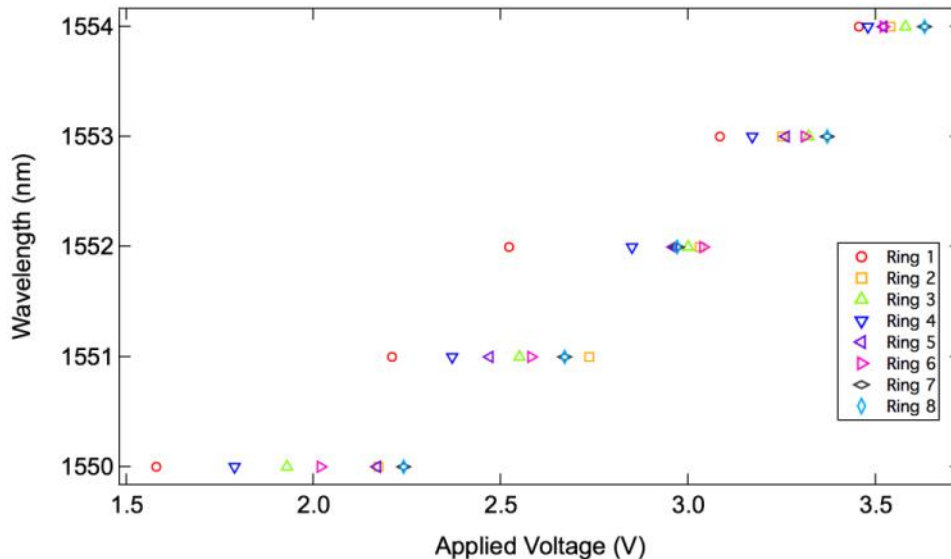


Fig. 5. Resonance wavelength vs applied voltage to the ring heaters. The resonance wavelengths are spread out more at low voltages than at higher ones. This happens because the ring resonances are separated by a fixed amount in wavelength from fabrication. Since the temperature of the rings depends on the power dissipated by the heaters, the shift in resonance wavelength goes as the square of the voltage. A small difference in resonant wavelength represents a larger difference in voltage at lower voltages than at higher ones.

We achieve tunable delays between 2 and 187 ps. We tune the resonance detuning of the two sets of resonators by adjusting the voltages supplied to the heaters. When the resonant wavelengths of all eight resonators coincide with the signal wavelength, i.e., the case of no detuning, we observe a delay of 187 ps. When we separate the resonances by 5 GHz, the

delay is reduced to 169 ps. For a resonance detuning of 10 GHz we measure a delay of 135 ps. As we continue to increase the resonance shift, the measured delay continuously decreases. The measured NRZ waveforms for the different delays are shown in Fig. 6a, starting with a reference waveform when the resonances are moved away from the operating wavelength, providing a zero delay trace, through delays of 9 ps (50 GHz detuning) up to 187 ps (no detuning). The smallest delay we measure is 2 ps, for a detuning of 60 GHz, shown in Fig. 6b, which compares the measured delay versus detuning frequency. Figure 6b also includes a curve for the simulated time delay versus resonance detuning, which provides a good match with experimental results. The simulated curve is generated using the equations from Ref. 27. As expected, all waveforms in Fig. 6a in which the balanced SCISSOR operation is used (resonators detuned), show delayed versions of the reference waveform with little to no distortion. The waveform for zero detuning shows clear distortion, with small oscillations seen in the '1' levels for all other waveforms not seen in this case. This distortion is due to the narrow bandwidth obtained when all resonances are aligned, as shown in Fig. 1 (I). Significantly longer delays can be achieved by simply increasing the number of rings in the device. We observed approximately 3.2 dB of loss due to the delay line for the 94 ps delay case, which corresponds to a propagation loss in the rings of 4.5 dB/cm or 0.028 dB loss per round trip in one ring.

The power consumption of the device is below 30 mW, which is the amount of power (calculated from the power supply voltage and current) that was being drawn from the DC power supply used to drive all the heaters. To first order, the power consumption of the device depends directly on the bias voltage applied to the rings to bring them to the operating wavelength, because the rings' resonances are then evenly split around the bias point. Thus, reducing the bias required to operate the device will lower its power consumption.

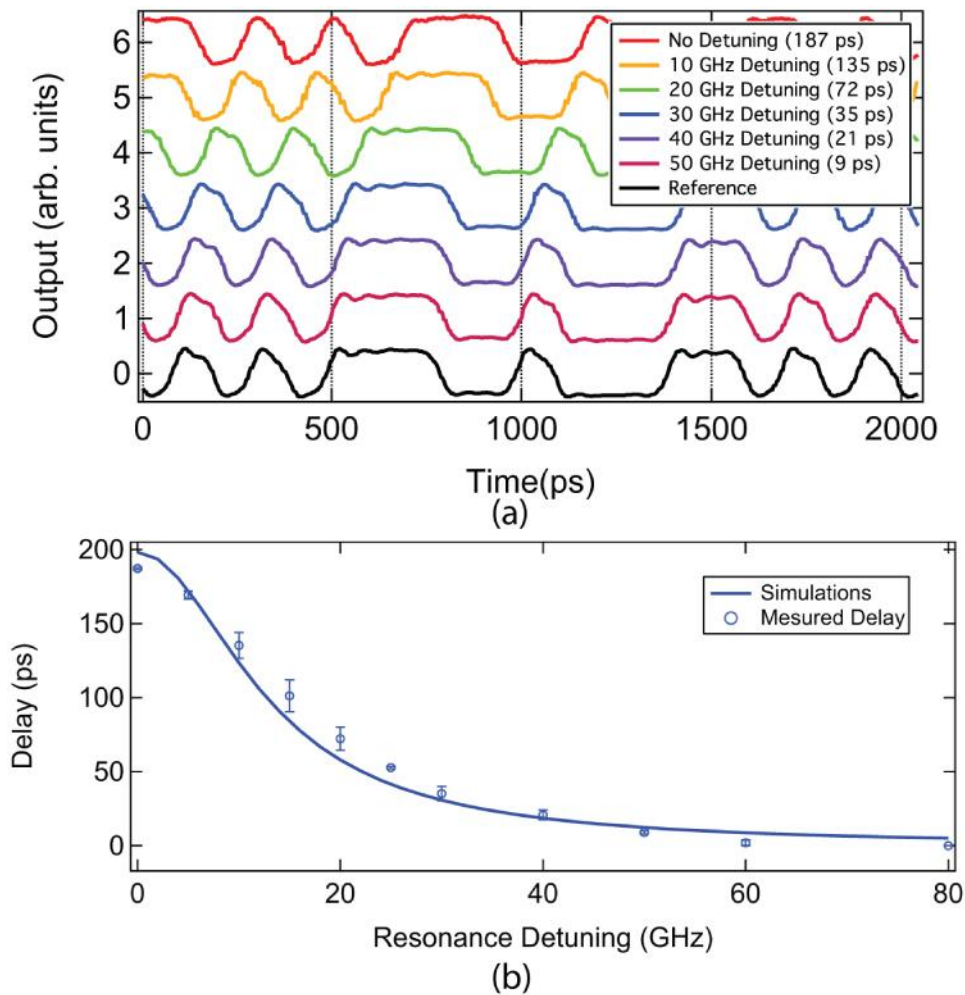


Fig. 6. Delay results of the 8 ring balanced SCISSOR. (a) Oscilloscope traces showing the signal output for the different resonant frequency detuning. (b) Delay as a function of resonant frequency detuning (measured delay noted in parenthesis). The solid line is the simulated delay.

The delay is continuously tunable, limited only by the smallest voltage change that can be applied. From Fig. 5 we find that the slope of the curve about the operating wavelength for the rings, 1551 nm, has an average of 0.477 V/nm. Considering a change of 1 mV as the minimum voltage change, one can tune the resonances in wavelength steps of 2.1 pm. From Fig. 5, we obtain that the slope of the delay versus resonance detuning is 6.3 ps/GHz around 1551 nm wavelength. Therefore, the minimum tunable time step size in this case is 1.6 ps.

To further illustrate that the tunable delay in the balanced SCISSOR is essentially distortion free, we measure the BER for the device as we vary the delay. A $2^{31}-1$ pseudorandom bit sequence is sent through the device and we measure the error rate at the receiver. The BER curves in Fig. 7 show that for a resonance detuning of 10 GHz or greater (corresponding to a delay of 135 ps or less), the power penalty from the delay is very small, within our measurement error. When all the rings are on resonance, (i.e. the rings are not in the balanced SCISSOR configuration and third order dispersion isn't cancelled) the power penalty becomes large, approximately 3 dB. The power penalty decreases to about 2 dB for a resonance detuning of 5 GHz (delay of 169 ps) indicating that the distortion introduced by the

third order dispersion in the delay line is reduced and that the bandwidth is clearly increased in the balanced SCISSOR. As predicted in the simulations (Fig. 2b), when the resonance detuning is set to 10 GHz or more, the third order dispersion is effectively canceled and the BER penalty is negligible.

The maximum tunable delay-bandwidth product is approximately 0.18 per ring, significantly larger than the 0.11 per ring result attained for the same 10 Gbps bit rate in [17]. Our scheme is comparatively simple, since, in principle, it does not necessarily require individually tunable resonance shifts for each ring (limited by fabrication tolerances). As we observe very little deterioration of the signal it appears that nearly the same distortion-free delay may be attained even at 40 Gbps using the balanced SCISSOR scheme. The results confirm the observation made in [27] that reducing the lowest (third) order contribution to the group delay dispersion is critical, and that trying to further flatten the delay characteristics can lead to additional complexity with a diminishing payoff.

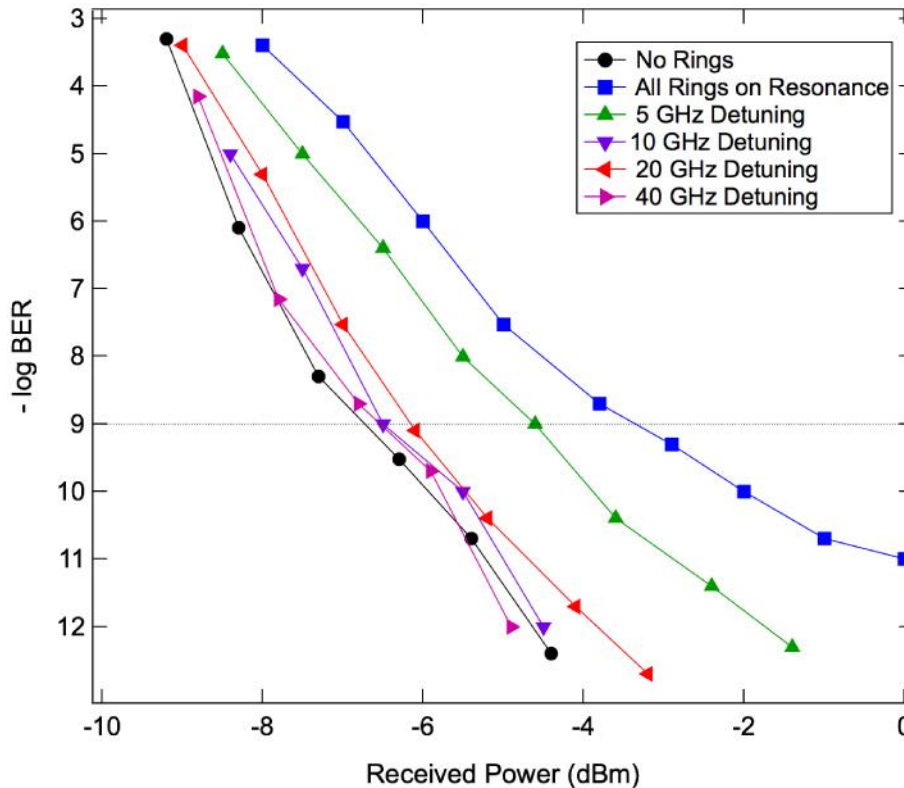


Fig. 7. Bit error rate measurements for different resonance detuning. For a detuning of 10 GHz or greater, the power penalty for the delay becomes very small.

5. Conclusion

In summary, we demonstrate here a continuously tunable delay based on silicon microring resonators in a novel balanced SCISSOR configuration, characterized by low group delay dispersion and low loss. The delay is tuned with localized heaters fabricated on top of the microrings. We show distortion free operation for the delay of a 10 Gbps signal, tunable between 2 and 135 ps. This range can be expanded by increasing the number of rings in the device. The minimum tuning step size is only limited by the minimum voltage increment that can be applied to the heaters, providing 1.6 ps for a 1mV step, and the low distortion indicates that both longer delays and wider bandwidth can be achieved in a CMOS-compatible balanced SCISSOR device.

Acknowledgments

The authors would like to thank John R. Lowell from Defense Advanced Research Projects Agency (DARPA) for supporting this work under the DARPA Slow-Light Program and Morton Photonics for supporting this work under DARPA SBIR contract # W31P4Q-09-C-0298, "Highly-Integrable Microresonators with Fast Tunable Group Delay for Broadband RF True Time Delay". This work was performed in part at the Cornell NanoScale Facility, a member of the National Nanotechnology Infrastructure Network, which is supported by the National Science Foundation (Grant ECS-0335765).